Journal of Experimental Zoology Part B: Molecular and Developmental Evolution

WILEY

JEZ-B MOLECULAR AND DEVELOPMENTAL EVOLUTION

RESEARCH ARTICLE OPEN ACCESS

A Morphospace Exploration Using a General Model of Development Reveals a Basic Set of Morphologies for Early Animal Development and Evolution

Hugo Cano-Fernández[1] | Miguel Brun-Usan[2] | Tazzio Tissot[3] | Isaac Salazar-Ciudad[1,4]

[1]Genomics, Bioinformatics and Evolution Group, Departament de Genètica I Microbiologia, Universitat Autònoma de Barcelona, Cerdanyola del Vallès, Spain | [2]Departamento de Paleobiología, Center for the Integration of Paleobiology, Universidad Autónoma de Madrid, Madrid, Spain | [3]Electronics and Computer Science Department, University of Southampton, Southampton, UK | [4]Centre de Recerca Matemàtica (CRM), Cerdanyola del Vallès, Spain

Correspondence: Hugo Cano-Fernández (hugo.cano@uab.cat)

Received: 6 June 2024 | **Revised:** 16 October 2024 | **Accepted:** 1 November 2024

Funding: The study was supported by the Spanish Ministry of Science and Innovation for funding (PID2021-122930NB-I00 and CNS2022-135397) to I.S.-C. and FPU19/01428 to H.C.-F. This work was also supported by the Spanish State Research Agency, through the Severo Ochoa and María de Maeztu Program for Centers and Units of Excellence in R&D (CEX2020-001084-M) to the Centre de Recerca Matemàtica.

Keywords: early animal development | evolution | modeling | morphogenetic transformation | morphology

ABSTRACT

What morphologies are more likely to appear during evolution is a central question in zoology. Here we offer a novel approach to this question based on first developmental principles. We assumed that morphogenesis results from the genetic regulation of cell properties and behaviors (adhesion, contraction, etc.). We used EmbryoMaker, a general model of development that can simulate any gene network regulating cell properties and behaviors, the mechanical interactions and signaling between cells and the morphologies arising from those. We created spherical initial conditions with anterior and dorsal territories. We performed simulations changing the cell properties and behaviors regulated in these territories to explore which morphologies may have been possible. Thus, we obtained a set of the most basic animal morphologies that can be developmentally possible assuming very simple induction and morphogenesis. Our simulations suggest that elongation, invagination, evagination, condensation and anisotropic growth are the morphogenetic transformations more likely to appear from changes in cell properties and behaviors. We also found some parallels between our simulations and the morphologies of simple animals, some early stages of animal development and fossils attributed to early animals.

1 | Introduction

What morphologies are more likely, or even possible, to appear during animal evolution is a central question in both zoology and evolutionary biology. Evolutionary developmental biology (or evo-devo) proposes that there are two processes we must take into account to answer this question. The first one, the generative processes, is what morphologies can be produced by development in a given population and generation. The second one, the selective processes, is which of those morphologies can survive and reproduce in their environment and, thus pass to the next generation (Salazar-Ciudad and Cano-Fernández 2023). This article focused on the generative process of morphology, development, and it aimed to determine what morphologies are more likely to appear in early animal development.

Morphology can be defined as the distribution of cells and extracellular matrix in space. Development is the process that generates morphology and can be seen as the spatio-temporal coordination of two subprocesses: induction and morphogenesis (Salazar-Ciudad, Jernvall, and Newman 2003).

Induction involves cells sending extracellular signals to each other, or receiving signals from the external environment, and as a result changing their gene expression, and eventually their cell type. Induction results in spatial patterns in the distribution of cell types or gene expression in space but, importantly, it does not change by itself the position of the cells (Salazar-Ciudad, Garcia-Fernández, and Solé 2000).

In morphogenesis, cells modify their distribution in space as a result of the physical forces produced by changes in their biomechanical properties (e.g. adhesion, shape, etc.) or the regulation of cell behaviors (e.g. cell division, apoptosis, etc.) (Alberch 1991; Salazar-Ciudad, Jernvall, and Newman 2003). In this study, a particular change in the relative positions of cells in space (e.g. folding, elongation, etc.) is defined as a *morphogenetic transformation*. It is important to note that the same morphogenetic transformation can produce slightly different morphologies depending on its intensity. For example, two invaginations can be considered the same morphogenetic transformation in spite of having different curvature (Gilbert 2019). Moreover, we did not considered isotropic growth (i.e. growth maintaining the same shape) as a morphogenetic transformation.

Induction and morphogenesis are not completely independent processes. Morphogenetic transformations are often triggered by changes in gene expression (Alberch 1991). Moreover, the spatial distribution of cells affects the diffusion of extracellular signals and, thus, the spatial distribution of the cells receiving such signals. A morphogenetic transformation can, therefore, lead to a change in gene expression (Salazar-Ciudad 2006, 2010).

In this article, we explored the space of possible morphologies, or morphospace, that can develop from very simple assumptions regarding both induction and morphogenesis. To do this, we used EmbryoMaker, a computational model of development, that allows to simulate organisms composed of epithelial and mesenchymal cells that are able to regulate the aforementioned cell properties and behaviors (Figure 1). To obtain a comprehensive sample of possible morphologies, we used EmbryoMaker in two different approaches.

In the ensemble approach, we performed a large number of simulations where cell properties and behaviors were regulated in simple territories (gradients or stripes) within spherical initial conditions we named blastuloids (see methods for a

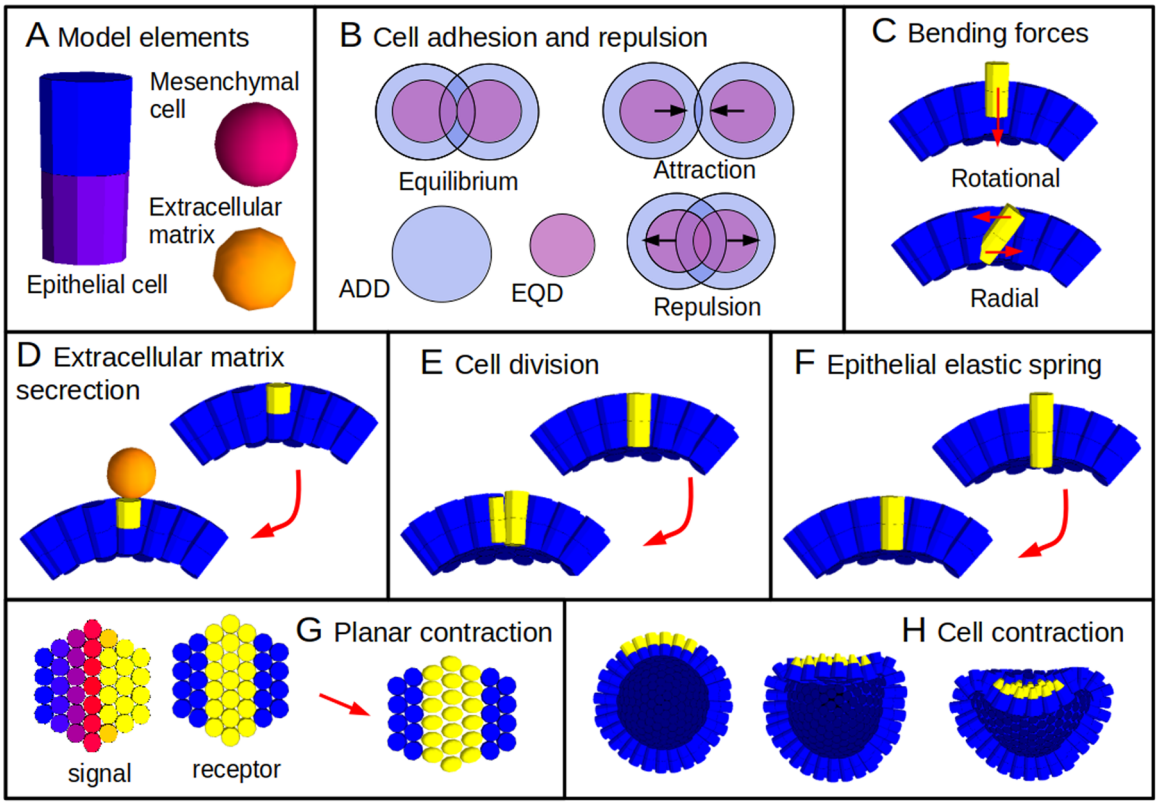

FIGURE 1 | EmbryoMaker. (A) Types of model mechanical elements. Epithelial cells are simulated as cylinders, mesenchymal cells and extracellular matrix are simulated as spheres. (B) Cell adhesion and repulsion. If the distance between two nodes is smaller than their equilibrium distances (EQD) they suffer repulsion and if it is larger (but still in the range of their adhesion radii, ADD), they suffer attraction. (C) Bending forces. Rotational bending force precludes cells from moving up or down the epithelial layer and the radial bending force maintains epithelial cells parallel to each other. (D) Extracellular matrix secretion. A cell (in yellow) secretes a new extracellular matrix node (orange sphere). (E) Cell division. New cells initially appear as smaller cylinders that progressively grow. (F) Epithelial elastic spring. The apical and basal nodes of epithelial cells are connected by an elastic spring. (G) Planar contraction. Cells can change their shape by contraction in one direction and expanding in another within the plane of the epithelium. This polarization is in the direction of the gradient of a growth factor in space. The same mechanism is used to simulate polarized contraction in mesenchymal cells. (H) Cell contraction in the apical–basal axis. The equilibrium distance and adhesion radius of the yellow nodes became smaller (or larger) due to changes in the genes expressed in it, as a result the epithelium invaginates.

complete description of these) that grew homogeneously by cell division simulating the presence of nutrients. A *territory* is defined as a set of cells that have something in common (e.g. the expression of a particular gene) and have a specific continuous distribution over space (Salazar-Ciudad, Jernvall, and Newman 2003). These territories were placed along two orthogonal axes, that were called the anterio-posterior and dorso-ventral axes in accordance with the early development of many animals. Moreover, initial conditions were spherical because that is a common shape in the early development of animals (e.g. cnidarian blastula) (Gilbert 2019).

In the focal approach, we performed simulations in the same blastuloids but slightly more complex developmental settings. The aim of this approach was to to explore further some aspects of the morphogenetic transformations and the results of the mechanical interactions between epithelium and mesenchyme.

Overall, our article explored the range of morphogenetic transformations that are most easy to produce by the simple regulation of the behaviors and mechanical properties of animal cells. Consequently, we obtained a basic set morphologies that are likely to appear during evolution in animals. For each morphogenetic transformation we explore the different underlying cell behaviors and cell mechanical properties (e.g., the different ways to produce invaginations by regulating different cell behaviors and mechanical properties). Within this set of morphologies, we found those of some simple living animals, early developmental stages of more complex animals and some fossils attributed to early multicellular animals (see discussion).

2 | Materials and Methods

2.1 | The Model

EmbryoMaker is a mathematical model that can simulate the development of organisms and organs composed of epithelial cells, mesenchymal cells and extracellular matrix (ECM). A more detailed description of EmbryoMaker can be found in its original publication (Marin-Riera et al. 2015) and the most updated version of the code is freely available online (https://github.com/HugoCanoFernandez/Morphospace_exploration_EMaker/tree/main/EmbryoMaker).

Cells in EmbryoMaker are simulated as sets of nodes that have some physical properties and gene expression levels. For the sake of simplicity, in this study epithelial cells were simulated as cylinders with two nodes: apical and basal. Apical nodes were located towards the outside of the blastuloid and basal nodes towards the inside. Conversely, mesenchymal cells and ECM were simulated as spherical nodes (Figure 1A). All nodes have the following mechanical properties: adhesion radius (p^{ADD}), equilibrium distance (p^{EQD}), adhesion (p^{ADH}) and compressiblity (p^{REC}).

The adhesion radius and equilibrium distance of nodes represent their size and, therefore, the size of cells. The size and relative position of nodes determine their biomechanical interactions. If two nodes are within their adhesion radius they attract each other, but if they are closer than their equilibrium distance they repel each other (Figure 1B). The strength of these forces is determined by the distance between the nodes and their adhesion and compressibility coefficients. These two parameters represent the amount and affinity of the adhesive molecules (e.g. cadherins) present in the cell membranes and the compressibility of cytoplasm.

Epithelial cells have some extra properties, namely: the equilibrium distance of the spring (p^{EQS}) the Hooke's constant (p^{HOO}) and the rotational (p^{EST}) and radial (p^{ERP}) bending forces. The cylindrical shape of epithelial cells is modeled using two nodes linked by a spring that represents the cytoplasm connecting them. The preferred length of this spring (i.e. the height of the relaxed epithelium) is its equilibrium distance (p^{EQS}). If the distance between the upper and lower nodes is larger than p^{EQS}, then they suffer an attraction force and if it is smaller, then there is a repulsion force (Figure 1F). The strength of these interactions is determined by the Hooke's constant of the spring (p^{HOO}). Epithelial cells also present bending forces (Figure 1C), that try to maintain the physical integrity of the epithelial layer by precluding cells from protruding from the plane of the epithelium (p^{EST}) and by maintaining the longest axes of the neighboring cells parallel (p^{ERP}).

Finally, cells in EmbryoMaker are able to perform the main cell behaviors that, according to phylogenetic analysis (see Section 1), were possible in the first multicellular animals: cell division, cell contraction, cell growth, and ECM secretion. Cell division is simulated adding a new cell next to the parental one (Figure 1E) at a rate named C_k. New cells start being very small and they grow until reaching the size of the parental one. They also inherit all the physical properties from their parental cells. Cell contraction (p^{COD}) and cell growth (p^{GRD}) are simulated as changes in the node equilibrium distance (Figure 1H). Cell contraction can also be polarized in the direction of some spatial gradient. In epithelial cells this means that they can elongate in a specific direction within the plane of the epithelium (Figure 1G), whereas mesenchymal cells can be polarized and contract in any direction. In ECM secretion, a new ECM node is secreted by the cells with a rate equal to the parameter p^{ECM} (Figure 1D). All these properties and behaviors are subject to genetic regulation (see below). See Supplementary Tables S1-3 for a complete list of the parameters used and the range of values considered.

2.2 | Initial Conditions

In this study, we assumed spherical initial conditions with patterns in form of gradients and/or stripes. We assumed that these territories were the result of a process of induction, either by extracellular cell signaling or by changes in the environment (see Section 1), although we did not simulated the induction process itself. We call these initial conditions blastuloids, because of their reminiscence to the blastulae of the early developmental stages of many extant animals. Also for the sake of simplicity and symmetry, all cells in the blastuloids are assumed to divide with a constant basal rate ($C_k = 0.5$) to simulate the growth of the organism due to the presence of nutrients.

Three different blastuloids, each one featuring a different distribution of cell types and a different configuration of territories,

were used as initial conditions for our simulations. For the sake of simplicity, we used the terms of anterior, posterior, dorsal and ventral to describe the orthogonal axis of the spheres (Figure 2), just as in animal embryos (Gilbert 2019).

The first initial condition (IC1) was a hollow sphere of epithelial cells (372 cells) with two slightly overlapping gradient territories. One gradient increased from the posterior towards the anterior pole of the embryo and the other from the ventral towards the dorsal area (Figure 2A–E). The simulations using this hollow blastuloid were used to understand the effects of the different cell properties and behaviors in the epithelial tissue alone. This initial condition offered a default expectation of the morphogenetic transformations that could have happened if the blastuloids were full of a material mechanically similar to the external medium, meaning that the internal and external pressures were equivalent.

The second initial condition (IC2) was an epithelial sphere full of mesenchymal cells (372 epithelial cells and 400 mesenchymal ones) with four gradient territories (Figure 2F–K). Two of them were in epithelial cells in the epithelium as in IC1. The other two were obtained by mirroring these epithelial territories in the underlying mesenchymal cells. This initial condition was used to study the mechanical interactions between epithelial and mesenchymal tissue during morphogenesis. In other words, the simulations with IC2 allowed to determine how the presence of mesenchymal cells can affect the morphogenetic transformations in the epithelium. To preclude the breakage of the epithelium due to internal pressure, mesenchymal cells divided in IC2 with a slower background rate than the epithelial ones ($C_k = 0.5$ for epithelial cells and $C_k = 0.25$ for mesenchymal ones). Therefore, the mesenchyme only produced some internal pressure at the first stages of development.

The third initial condition (IC3) had the same spatial distribution of cells that IC2, but with three striped territories of homogeneous expression in mesenchymal cells (Figure 2L–P). These territories were placed in the anterior pole, the posterior pole and the equator of the embryo, simulating a french-flag pattern that can be easily obtained from an environmental gradient or a reaction-diffusion system (Salazar-Ciudad 2006). On the contrary, epithelial cells showed no distinct territories. This IC3 setting was used to study the morphogenetic transformations that are possible in the mesenchyme. The background division rates were the same as in IC2.

2.3 | Ensembles

We explored the ensemble of morphologies that can develop from these initial conditions by regulating different cell properties and/or behaviors in each initial territory in the blastuloid. We exhaustively tried all combinations of cell behaviors and properties in different territories, including the possibility of inactive territories (i.e. not activating any cell property of behavior). For example, in the initial conditions with two territories (IC1) we tried the combinations: anterior territory contracting and dorsal territory inactive, anterior territory inactive and dorsal territory contracting, anterior territory contracting and dorsal secreting ECM, anterior territory secreting ECM and dorsal contracting, and so on. We used one value for the regulation of each cell property or behavior. Those values can be consulted in Table S3. In total, we performed 257 simulations from IC1, 5621 simulations from IC2 and 256 simulations from IC3. The simulations were performed for 10 time units of the model, which roughly corresponds to 10,000 iterations, using 4th- order Runge-Kutta numerical integration method with a dynamic step size (Marin-Riera et al. 2015).

2.4 | Quantitative Measurements

The morphogenetic transformations found in the simulations were also measured quantitatively. Folding in the epithelium was quantified by calculating the average distance to the center of the morphology in the cells of the invaginated or evaginated territory minus the average distance to the center of the morphology of all the cells. In a regular sphere this value should be equal to 0 in all cells. In cells from a territory that is evaginated, however, this value is larger than 0, and in cells from a territory that is invaginated, it is smaller than 0.

Elongation both in the mesenchyme and the epithelium was quantified by calculating the largest distance between two cells in the three axes of the blastuloid: anterior–posterior, dorsal–ventral and right-left. The elongation coefficient in one axis was calculated by dividing the distance in that axis by the larger distance of the other two. This elongation coefficient was equal to 1 if the morphology remained spherical and larger than 1 if it was elongated.

Condensations in the mesenchyme were quantified by measuring the average distance of each cell to its neighbors and the total number of neighbors. Cells in condensations have a smaller average distance to their neighbors and also more neighbors.

3 | Results

3.1 | Morphogenesis in the Epithelium

We simulated development from IC1, a spherical epithelial blastuloid (Figure 2). In each simulation we regulated a different combination of cell behaviors and cell mechanical properties. All the morphological transformations occurring in these simulations can be classified into only three types: elongation, evagination and invagination. Elongation happened when the otherwise spherical blastuloid became an ellipsoid. Evaginations and invaginations were, respectively, outwards or inwards folds of the blastuloid surface. Evaginations and invaginations can actually be considered as a single morphogenetic transformation, that is, folding. In IC1 we considered two territories where cell properties and behaviors could be regulated differently (Figure 2). When two different cell properties or behaviors were activated in these territories, the resulting morphology could be described as the combination of two morphogenetic transformations (e.g. evagination in the animal territory and invagination in the dorsal territory). A depiction of the range of morphologies that was obtained from

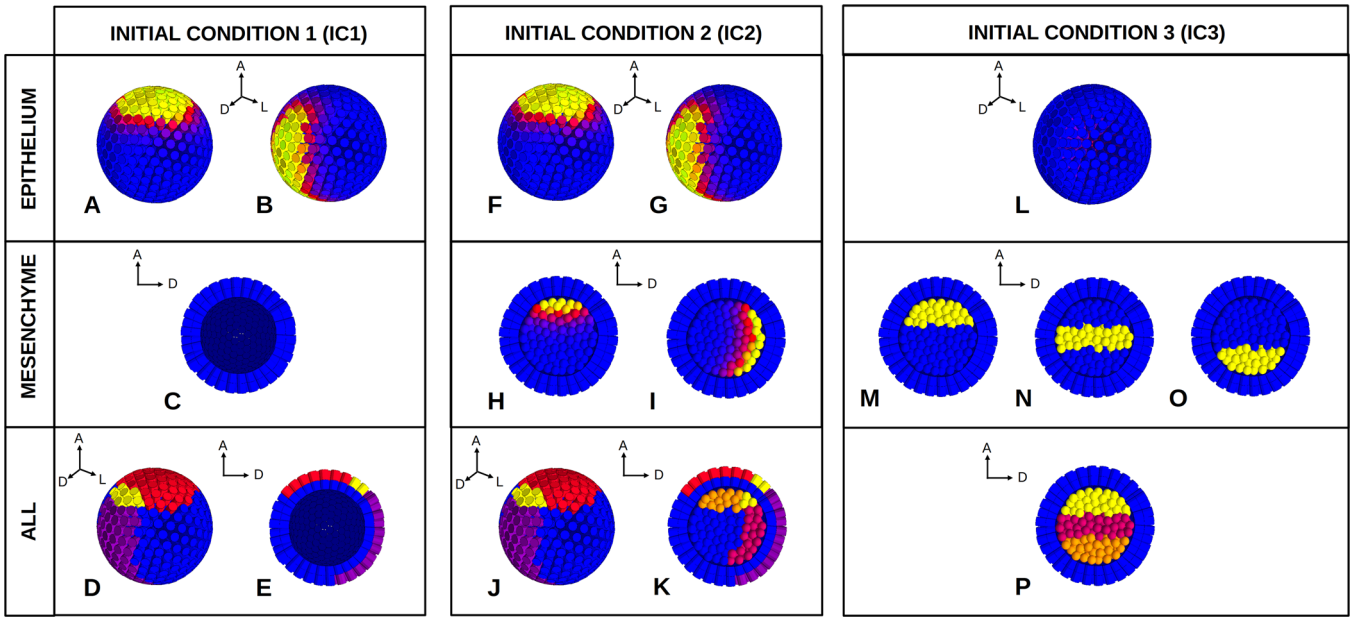

FIGURE 2 | Initial conditions. Each of the three panels shows one initial condition. The first row in the panels shows the territories in the epithelium and the second the territories in the mesenchyme. The colors in the two first rows show the relative activation strength of the properties and behaviors, meaning that cells in yellow activate them with the highest value and cells in blue do not activate them. In other words, the colors can represent either the expression of a gene or a change in environmental conditions (e.g., light, nutrients) heterogeneous in space. The third row shows a combined map of the territories both in epithelium and mesenchyme, where cells with an activation strength of at least 30% of the maximum value are painted with the same color. Cells that can activate two cell properties or behaviors with a strength higher or equal to this threshold are painted in yellow. A stands for anterior, L for lateral right and D for dorsal. (IC1, A–E) Hollow epithelial sphere with two territories, one in the anterior pole and the other in a dorsal stripe. (IC2, F–K) Epithelial sphere full of mesenchymal cells with four territories, two in the epithelium and two in the mesenchyme. (IC3, L–P) Epithelial sphere full of mesenchymal cells with three territories in the mesenchyme.

all these combinations of morphogenetic transformations is shown in Figure 3 (i.e. all combinations of evaginations, invaginations and elongation). The relationships between the morphogenetic transformations and the cell properties and behaviors that produced them are presented in Table 1.

3.1.1 | Elongation

In our simulations, elongation was only observed when planar cell contraction was active (Table 1). The mechanistic explanation of this result is that cells contracting within the plane of the epithelium become more elongated in a specific direction (Figure 1G), thus contributing to the overall elongation (Figure 3).

3.1.2 | Evagination

In contrast, the regulation of many cell properties and behaviors led to evaginations (Figure 4A–E and S1.A–E and Table 1). The behavior that produced the largest evaginations was basal cellular contraction (p^{COD}). This behavior changed the shape of epithelial cells from cylindrical to conical. In these conical cells, the apical node (the one facing the outside of the blastuloid) was larger than the basal node (the one facing the inside). In real epithelial cells, this can be achieved by the contraction and relaxation of the actomyosin bands in their cytoskeleton (Martin, Kaschube, and Wieschaus 2009; Pearl, Li, and Green 2017). This change of cell shape increased the local curvature of the territory outwards thus producing an evagination. Evaginations also arose when increasing the size (equilibrium distance or p^{EQD}) of the apical nodes in epithelial cells by cell growth (p^{GRD}).

A local reduction in the epithelial thickness also resulted in evaginations. Epithelial thickness was reduced in our simulations by decreasing the height of epithelial cells (Figure 1C). Cell height was controlled by the equilibrium distance between the apical and basal nodes of epithelial cells (p^{EQS}). In animals, cells can reduce their cell height (i.e. cell shortening) by contracting their apicobasal actomyosin cable (Pearl, Li, and Green 2017), and it has been found that this produces folds in the ascidian gastrulation (Sherrard et al. 2010) and in *Drosophila* leg development (Monier et al. 2015).

Evaginations were also produced by decreasing cell compressibility or decreasing the adhesion affinity between cells. The epithelial nodes in EmbryoMaker have an equilibrium distance (p^{EQD}) and a maximum adhesion radius (p^{ADD}). When two nodes from different cells are within the range of their adhesion radii, they attract each other (Figure 1B). This attraction force depends positively on the distance between the nodes and on the property, p^{ADH}, that represents the adhesion affinity between cells. Conversely, when two nodes are at a distance smaller that the sum of their equilibrium distances, they repel each other (Figure 1B). This repulsion force depends negatively on the distance between the nodes and positively on their compressibility parameter, p^{REC}.

In our simulations the blastuloids had a background cell division rate. Each new cell meant more volume to be accommodated in

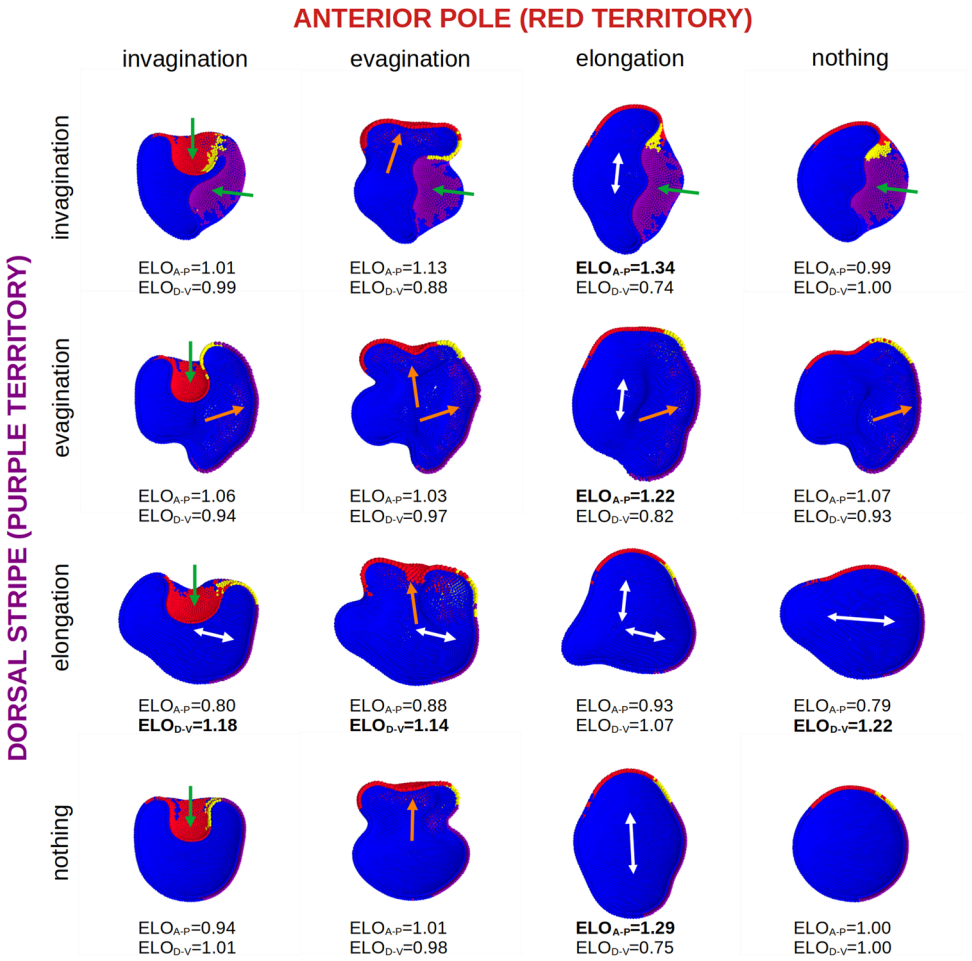

FIGURE 3 | Sample of morphologies obtained in the ensemble approach from the hollow blastuloid (IC1). In the simulations of this ensemble one cell property or behavior was regulated in each of the two territories (red or purple in the figure). We tried all the possible combinations of cells properties, behaviors in the two territories. For example, anterior territory contracting and dorsal territory inactive, anterior territory inactive and dorsal territory contracting, both territories inactive and both territories contracting. All the morphologies in this ensemble could be understood as the result of combining three morphogenetic transformations: invagination, evagination, and elongation. In this figure we show all these possible combinations. The columns represent the morphogenetic transformation present in the anterior pole territory (red). The rows represent the mechanical transformation present in the dorsal stripe territory (purple). The yellow cells represent the overlapping area between territories. The label "nothing" means that there were no cell properties or behaviors activated in that territory (i.e. inactive territory). The green arrows show invaginations, the orange arrows evaginations and the white arrows show the direction of elongation. Note that many cell properties or behaviors were able to produce invaginations or invaginations (see Table 1). The value "ELO" stands for the elongation coefficient in the anterior–posterior (A–P) and dorsal-ventral (D–V) axes (the calculations are explained in Section 2). For this figure we selected the results obtained regulating cell growth (p^{GRD}).

TABLE 1 | Morphological transformations produced when regulating (increasing or decreasing) cell properties and behaviors in IC1.

Property/behavior	Symbol	Increase	Decrease
Adhesion	p^{ADH}	Invagination	Evagination
Compressibility	p^{REC}	Evagination	Invagination
Adhesion radius	p^{ADD}	Invagination	Evagination
Cell contraction	p^{COD}	Evagination	Invagination
Cell growth	p^{GRD}	Evagination	Invagination
Cell high	p^{EQS}	Invagination	Evagination
Extracellular matrix secretion	p^{ECM}	Invagination	
Planar cell contraction	p^{PCO}	Elongation	

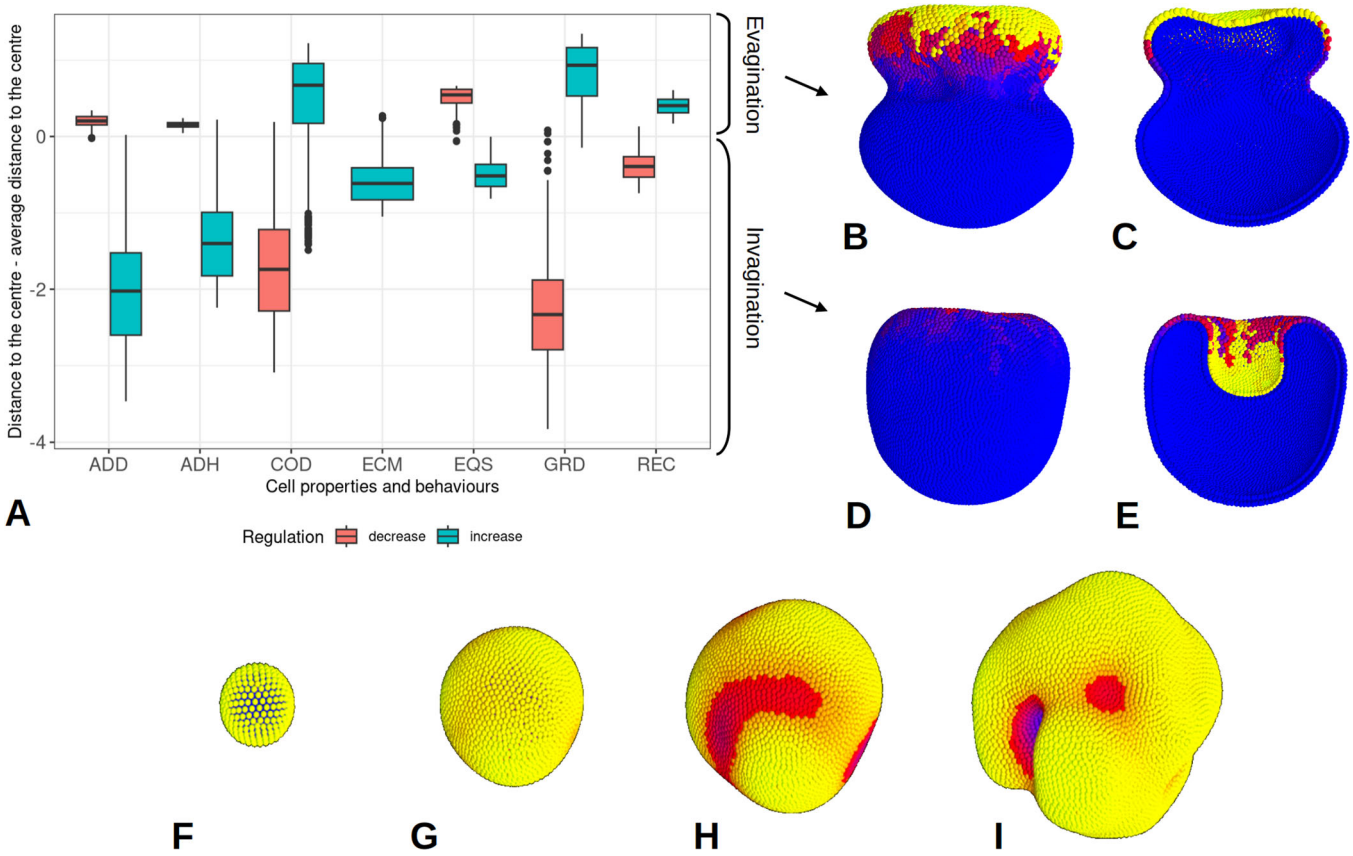

FIGURE 4 | Quantification of invaginations and evaginations in IC1 and condensations in IC3 ensemble simulations and random folds appearing in a focal approach simulation where IC1 grows by cell division. (A) Box-plot showing a quantitative evaluation of the invaginations and evaginations produced by the positive or negative regulation of various cell properties and behaviors in the ensemble simulations from IC1. ADD stands for adhesion radius, ADH for adhesivity, COD for cell contraction, ECM for extracellular matrix secretion, EQS for cell height, GRD for cell growth and REC for compressibility. Each box represents the cells of the anterior territory in one simulation where one cell property or behavior was activated in that territory (displayed in the *x*-axis). The colors of the boxes show whether the regulation was positive, increasing the value of the property or behavior, or negative, decreasing the value. The *y*-axis shows the distance to the center of the morphology in the cells from this anterior territory minus the average distance to the center of the morphology in all cells. In a perfect sphere, this value should be equal to 0. If this value is larger than 0, then it means that the territory has evaginated and if it is less than 0 then it has invaginated. In all the simulations of this figure, the dorsal territory remained inactive. (B) Lateral view of an example of an evagination produced by positive regulation cell growth (p^{GRD}), meaning that cells increase the size of their apical nodes. (C) Sagittal section of B. (D) Lateral view of an example of an invagination produced by negative regulation cell growth (p^{GRD}), meaning that cells decrease the size of their apical nodes. (E) Sagittal section of D. The color palette in (B)–(E) represents cell growth regulation with yellow representing the maximum value and blue representing no activation. (F–I) Different stages in a focal approach simulation of growth by cell division in IC1. The colors show the squared distance to the center of the blastuloid (yellow indicates the largest distances). The blastuloid grew from 372 cells (F) to more than 10 thousand cells (I).

the epithelium. New cells, therefore, produced strong repulsive forces with their neighboring cells and that resulted in the expansion of the blastuloid. In other words, to accommodate all this new volume, the blastuloids increased their size. The speed of this expansion depended on the relative strength of the repulsion and attraction forces between cells. If the compressibility of a territory was decreased (by increasing p^{REC}) then those cells expanded faster than the rest of the blastuloid creating an evagination. Similarly, when the adhesion affinity was decreased in a territory (p^{ADH}) the attraction forces keeping cell together were weaker, resulting in cells expanding faster than the rest of the blastuloid and creating an evagination.

Another way of producing evaginations was to reduce the adhesion radius, p^{ADD}. Notice this is different from the adhesion affinity (i.e. the strength by which cells attach to each other, p^{ADH}). The total strength of the forces sticking cells together was the sum of the attractive forces suffered by each pair of nodes that are within the range of their adhesion radii (Figure 1B). Reducing the adhesion radius of cells resulted in less pairs of nodes within the range of their adhesion radii and, therefore, less attractive forces. As explained before, when attractive forces were reduced in a territory these cells expanded faster than the rest of the blastuloid creating an evagination.

3.1.3 | Invagination

Invaginations were produced by the same processes described for evaginations, but activated in the opposite way (Figure 4A–E and Table 1). For example, invaginations were produced when

the size of the apical nodes were decreased by either cell growth or cell contraction (Figure 1H). Increasing the height of cells, decreasing their compressibility and increasing their adhesion affinity also produced invaginations. In the model adhesion affinity can be increased by increasing the parameter p^{ADH} whereas, in real tissues, this can happen when cells generate cytoplasm protrusions towards the outer or inner surface of the epithelium that drag neighboring cells. This mechanism is called bunching (Pearl, Li, and Green 2017) and it has been observed in the sea urchin gastrulation (Burke et al. 1991; Davidson et al. 1995).

Lastly, secreting ECM (p^{ECM}) towards the exterior of the blastuloid also produced invaginations because the repulsion forces between the ECM nodes and the apical epithelial nodes constrained the growth of the blastuloid in the areas where secretion was active. No evaginations were produced by ECM secretion in our simulations, but only because we did not allow ECM to be secreted to the interior of the blastuloid.

3.1.4 | Random Folding

The simulations of our focal approach showed that homogeneous growth by cell division can lead to randomly folded morphologies (Figure 4FR–I) particularly if division rate is high and/or the epithelium is very flexible (Hagolani et al. 2019; Cano-Fernández et al. 2024).

As mentioned above, cell division introduces new cells (Figure 1E) that increase in the volume of the epithelium. As a result, the cells in areas where there have recently been cell divisions are more compressed than the rest. Compressed cells produce strong lateral forces that are transmitted through the epithelium. These lateral forces can fold the epithelium either in the area where more new volume is accumulating or in the adjacent ones (Figure S2A,B). Although the cell division rate may be the same in all cells, not all of them divide exactly at the same moment.

Even when we forced cells to divide synchronously, random folds arose. We found that was due to the fact that each division plane has a specific direction. In other words, cells may divide in random directions within the plane of the epithelium but each cell divides in unique direction and, thus, leads, locally, to more pushing in this direction than in others. This results in some areas of the epithelium growing slightly more than others and this ultimately leads to the formation of folds. Notice that this cannot be precluded by forcing all cells to divide in the same direction within the plane of the epithelium. Geometrically, it is impossible that all cells at the surface of a sphere orient their division plane in the same direction. In our focal simulations with only cell division, therefore, the areas that have more or less extra volume are randomly located in the blastuloid, resulting in randomly located folds (Figure 4F–I).

More focal simulations were performed to confirm that the size and distribution of more compressed areas of the epithelium determines where these folds appear. The results of these simulations are in Supplementary text S1 and Figure S2.

3.2 | Morphogenesis in the Mesenchyme

The ensemble simulations from IC3 also exhibited a smaller number of morphogenetic transformations: condensation, anisotropic growth and elongation. However, by combining these transformations a wide range of configurations in the mesenchyme was obtained (Figure 5).

3.2.1 | Condensation

Condensations were regions of increased cell density that arose from the regulation of homotypic cell adhesion (Figure 6). Cells regulating homotypic adhesion adhere to each other stronger than to cells from other territories. In the model, this stronger adhesion arises simply from different cells expressing different adhesion molecules with different adhesion affinities.

A strong homotypic adhesion, therefore, aggregates neighboring cells from the same territory and precludes them from dispersing or mixing with cells of other territories, a phenomenon usually known as cell sorting. Cell sorting by differential adhesion has been observed in both in silico (Taylor et al. 2017; Cano-Fernández et al. 2023) and in vitro models (Steinberg 1970; Foty and Steinberg 2005; Lecuit and Lenne 2007). In fact, differential adhesion has been suggested as one of the mechanisms involved in the condensation of precartilage, for example, in animal limb development (Newman 1996).

3.3 | Anisotropic Growth

Mesenchymal growth happened in the ensemble simulations due to cell division. In isolation, growth by cell division resulted in an isotropic increase in the size of the mesenchyme and, therefore, could not be classified as a morphogenetic transformation (see definition in Section 1). However, when growth in some territories was combined with condensation in others, an increased growth be cell division led to anisotropic changes in the mesenchyme. For example, in simulations with two condensations separated by a non-condensed territory, growth in that territory determined the distance between the two condensations (Figure 5C).

3.3.1 | Elongation

Mesenchymal elongation was the result of the juxtaposition of multiple condensations in the ensemble simulations. In IC3, three mesenchymal territories were distributed as bands along the animal–posterior axis of the blastuloid (Figure 2M–P). When homotypic cell adhesion was regulated in these territories, multiple condensations were formed as explained before. Since these three territories were aligned along the A–P axis, the growth of the condensations resulted in an elongation of the blastuloid along the A–P axis, like in the somites in the segmentation of vertebrates (Figure 5C).

In our focal approach, we tested the ability of condensations to produce elongation in the whole blastuloid by increasing the

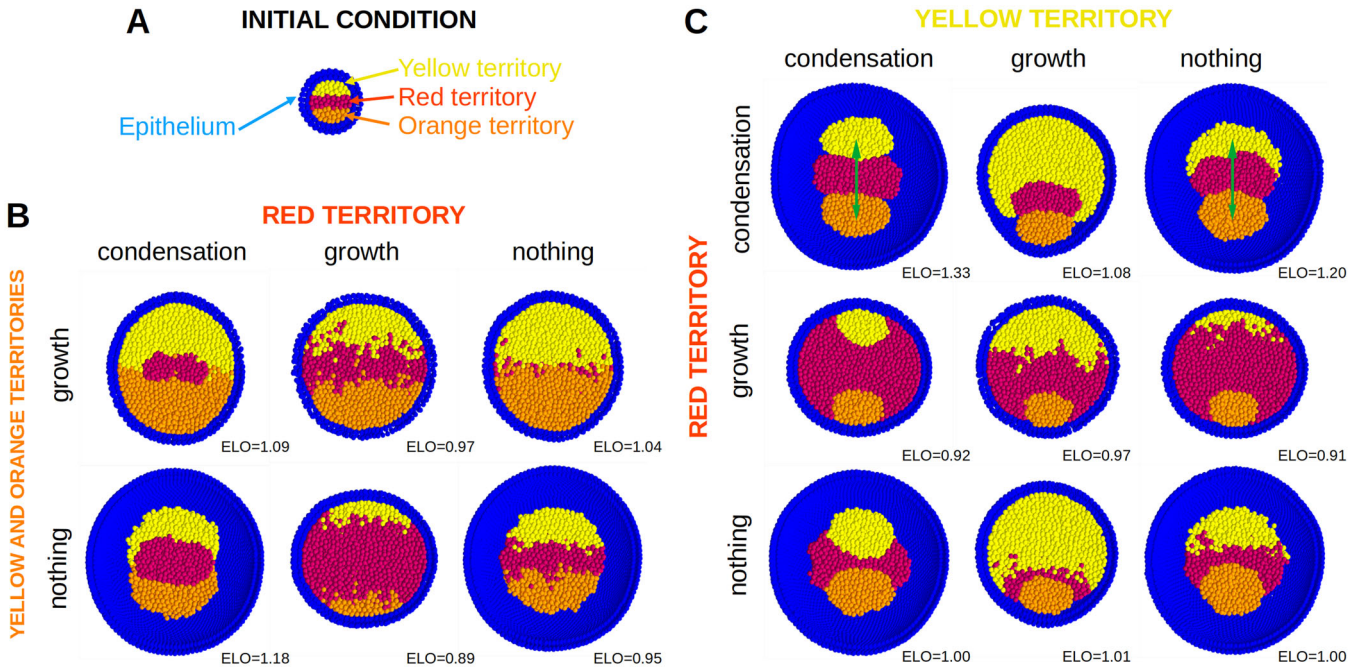

FIGURE 5 | The set of morphologies obtained in the ensemble from IC3 by combining condensation and anysotropic growth. (A) Sagittal section of the initial conditions showing epithelial and mesenchymal cells as spheres. Blue spheres are epithelial cells (each sphere represents either the apical or the lower node). Yellow, red, and orange spheres represent mesenchymal cells from the three territories where cell properties and behaviors (increased cell division that leads to tissue growth and homotypic adhesion or polarized cell contraction that lead to condensations) can be activated. (B) Sagittal sections of the morphologies obtained from all the possible combinations of increased cell division, condensation and just background cell division (nothing) assuming the orange and yellow territories activate the same cell property or behavior. (C) Sagittal sections of the morphologies obtained from all the possible combinations of increased cell division, condensation and just background cell division (nothing) assuming the orange territory activates homotypic adhesion (condensation). All the condensations in this figure were produced by homotypic adhesion, but similar results were obtained when activating polarized cell contraction. The value "ELO" stands for the elongation coefficient in the anterior–posterior axis (the calculations are explained in Section 2).

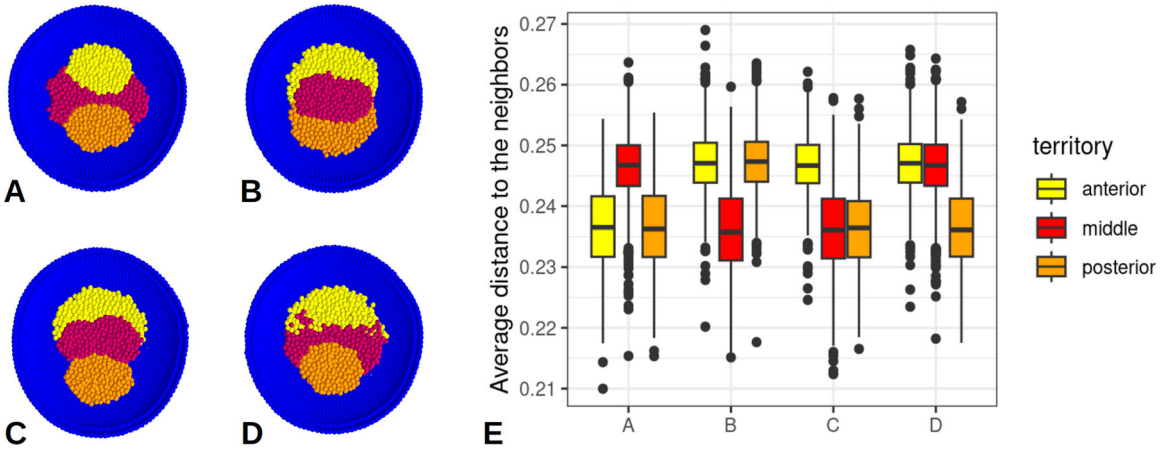

FIGURE 6 | Quantification of the mesenchymal condensations in ensemble simulations from IC3. (A–D) Examples of ensemble simulations with condensations from the IC3 in sagittal section. (A) Condensations in the anterior and posterior territories (yellow and orange). (B) Condensation in the middle territory (red). (C) Condensations in the posterior and middle territories (orange and red). (D) Condensation in the posterior territory (orange). (E) Box-plot showing a quantitative condensation produced by homotypic adhesion in the ensemble simulations from IC3. The *x*-axis represents the simulations (A–D). The boxes include the data from all mesenchymal cells in each territory (colors identify territories). The *y*-axis shows the average distance of mesenchymal cells to their neighbors.

number of areas along the anterior–posterior axis with enhanced homotypic adhesion and the division rate of mesenchymal cells. As expected, increasing the number of condensations effectively increased the total elongation of the blastuloid (Figure 7). However, the efficiency of this elongation process was limited by the initial number of mesenchymal cells. If the size of the initial conditions was maintained constant, adding many territories also meant that they had to be small. Small condensations expressing

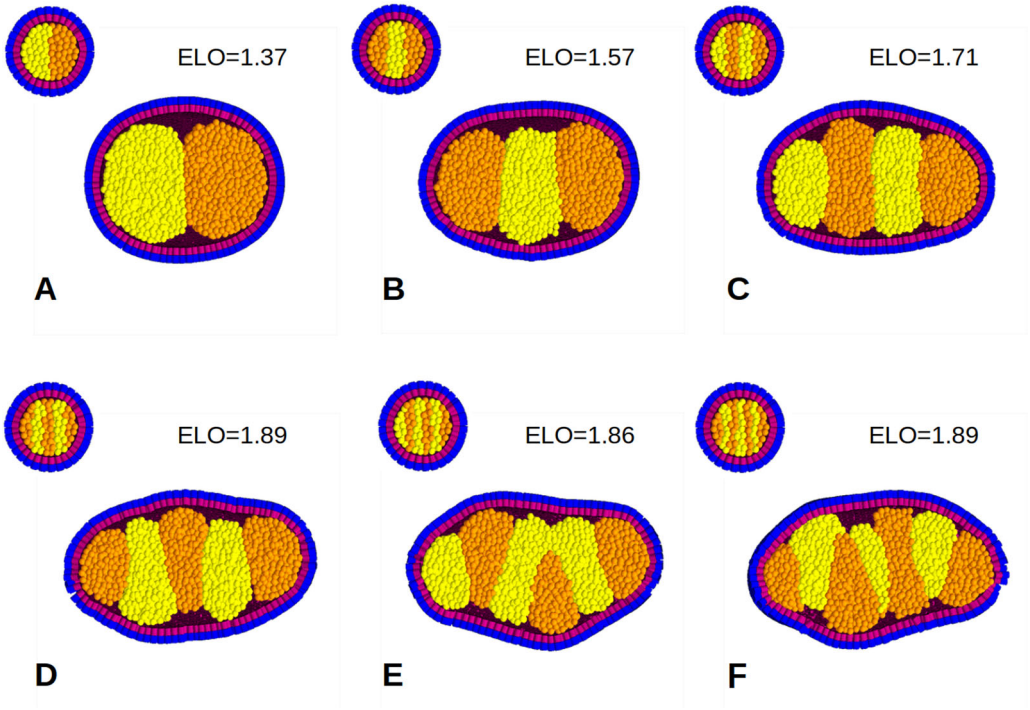

FIGURE 7 | Elongated morphologies obtained in the focal approach by the accumulation of mesenchymal condensations in one axis. (A–F) Sagittal sections of simulations with 2, 3, 4, 5, 6, and 7 initial territories in mesenchymal cells. Mesenchymal cells with the same color (either yellow or orange) suffer homotypic adhesion, meaning that they attract to each other stronger than to any other cell. For each simulation the initial condition is shown in the top left and final morphologies in the bottom right of the image. Note that, starting always from a spherical initial condition, the final morphology is more elongated the higher is the number of initial territories and therefore final mesenchymal condensations (or segments). The value "ELO" stands for the elongation coefficient in the longest (dorsal–ventral) axis (the calculations are explained in Section 2).

the same adhesion molecule were more likely to fuse totally or partially as shown in Figure 7E. Polarized cell contraction was also able to produce the elongation of the mesenchyme by itself, but it needed a constant signal diffusing from one point (e.g., the anterior pole) of the blastuloid (Figure S3).

3.4 | Morphogenetic Transformations Arising From the Mechanical Interaction Between Epithelium and Mesenchyme

The morphogenetic transformations resulting from changes in the properties of the epithelial cells differed between the initial condition IC1 (hollow epithelial sphere) and IC2 (epithelial sphere full of mesenchymal cells), even if the mesenchyme only grows by cell division without changing its properties or regulating any other behavior. For example, when epithelial cells in IC1 decreased their adhesion affinity (p^{ADH}) or adhesion radius (p^{ADD}) we obtained evaginations that were not replicated in IC2. This difference can be explained by considering that, at least at the first stages of development, mesenchymal cells adhere to epithelial ones and pull them towards the center of the blastuloid, thus precluding shallow evaginations from happening. Moreover, when the growth rate of the mesenchyme was increased, the internal pressure created by dividing mesenchymal cells pushed epithelial ones towards the exterior of the blastuloid, thus precluding invaginations (Figure S4).

Mesenchymal elongation, either by polarized cell contraction (Figure S3) or by the juxtaposition of condensed segments (Figure 7), also resulted in the elongation of the epithelium if the division rate of mesenchymal cells was high enough. The reason is that the growing mesenchyme produced higher repulsion forces in the axis of elongation, pushing epithelial cells further in that direction. This means that, when growing fast enough, the pressure exerted by the rapidly proliferating mesechyme can direct the growth of the epithelium that surrounds it.

Adhesion forces between mesenchymal and epithelial cells were also able to transform the epithelial morphology. This was also observed in our focal approach using an initial condition where mesenchymal cells adhered stronger to epithelial cells in the equator than to any other cell (Figure 8A–C). These simulations were repeated with different values of the division rate of mesenchymal cells. The results show that attraction forces from the mesenchymal cells can also transform the morphology of the epithelium. In these cases, the final morphology depends on the relative growth rates between the mesenchyme and the epithelium (Figure 8D–F). When the cell division rate in the mesenchyme was low, then they mesenchymal cells attracted epithelial cells in the equator enough to limit the expansion of the epithelium in that area. The result was an ellipsoid elongated along the anterior-posterior axis and with an equatorial layer of mesenchymal cells separating two internal cavities (Figure 8D). Conversely, when cell division rate in the mesenchyme was high, the mesenchyme grew towards the equator of the epithelial sphere because it is the direction where mesenchymal cells suffer more adhesion. In other words, epithelium, in this case, guided the growth of the mesenchyme, resulting in

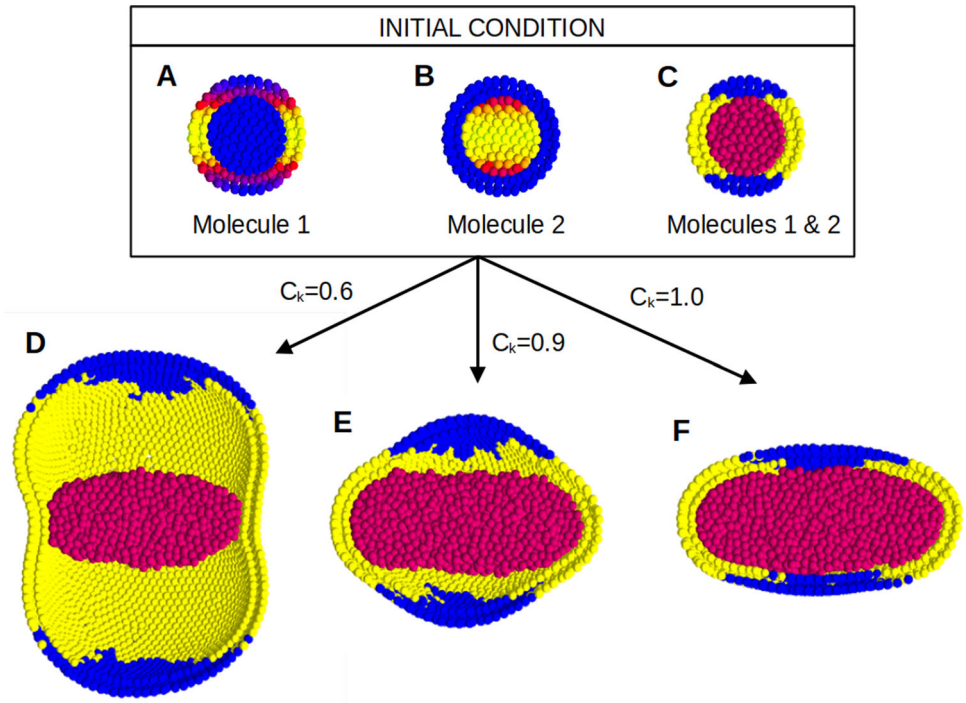

FIGURE 8 | Focal approach simulations showing that adhesion between mesenchymal and epithelial cells can produce morphogenesis depending on the growth rate in both tissues. (A–C) Sagittal section of the initial conditions showing a blastuloid full of mesenchymal cells. (A) Expression level (yellow means high and blue low concentration) of an adhesion molecule (molecule 1). (B) Expression level of a second adhesion molecule (molecule 2) that binds to the first one showed in A. (C) Expression level of both molecules, in yellow the cells expressing molecule 1 and in red the ones expressing molecule 2. (D–F) Morphologies that result from changing the background division rate (in cell division per hour) of mesenchymal cells (c_k) (D) $C_k = 0.6$ (E) $C_k = 0.9$ (F) $C_k = 1.0$. The background division rate of epithelium was $c_k = 0.5$. All the simulations were performed for 10 time units in the model from 772 cells to approximately 11000 cells.

a flat disk completely full of mesenchymal cells (Figure 8F). These results support the idea that the mesenchyme may have an active role in folding the epithelium as it has been suggested, for example, in the early development of the dental bud (Mammoto et al. 2011; Marin-Riera et al. 2018; Wang et al. 2022).

4 | Discussion

The results of our simulations showed that the morphogenetic transformations more likely to appear in development are invagination, evagination, elongation, and condensation. There are other morphogenetic transformations present in animals. For example, holes can be produced in the epithelium through the regulation of epithelial–mesenchymal transition or apoptosis. Moreover, mesenchymal cells can migrate, extend, and converge like, for example, in the gastrulation of many animals (Gilbert 2019). Mesenchymal cells can also produce cavities by changing the distribution of the adhesion molecules in their membranes and, eventually, transform into epithelial cells (Newman and Bhat 2008). This process has, indeed, been assumed in our initial condition IC1, which already presents an inner cavity. EmbryoMaker can also simulate migration, epithelial-mesenchymal transition and apoptosis but they were not included in this study for the sake of simplicity.

Our results also showed that the same morphogenetic transformation can be obtained by the regulation on many different cell properties and behaviors. For example, invaginations can be produced by changes in: cell contraction, adhesivity, compressibility, adhesion radius, cell growth, cell hight or ECM secretion (Table 1). Consequently, many animal lineages may have evolved similar morphologies but regulating different cell properties or behaviors, that is, evolutionary convergence (McGhee 2011). Moreover, some animal lineages can have retained their ancestral morphology during evolution but changed the cell properties or behaviors that are regulated to produce it, a phenomenon known as developmental systems drift (Newman and Müller 2000; True and Haag 2001).

In spite of the limited number of possible morphogenetic transformations (i.e. folds, elongations, etc.), our simulations reveal a wide range of variation, including morphologies that closely resemble the early developmental stages in extant animals as well as some fossils from early animals (Figure 9). In the next paragraphs, we will discuss some of these morphologies.

The gastrulation in cnidarians, for example, generally starts with a hollow sphere like our blastuloid (IC1). This sphere suffers an invagination that can be produced, depending on the species, by cell introgression (Hydrozoa) or by cell contraction (Anthozoa and Scyphozoa) (Technau 2020). Our simulations of invagination by cell contraction (Figures 9 and 4E) are similar to the former case. Invaginations by cell introgression, meaning that some cells detach from the epithelium and cover the interior of the blastula, can potentially be simulated in

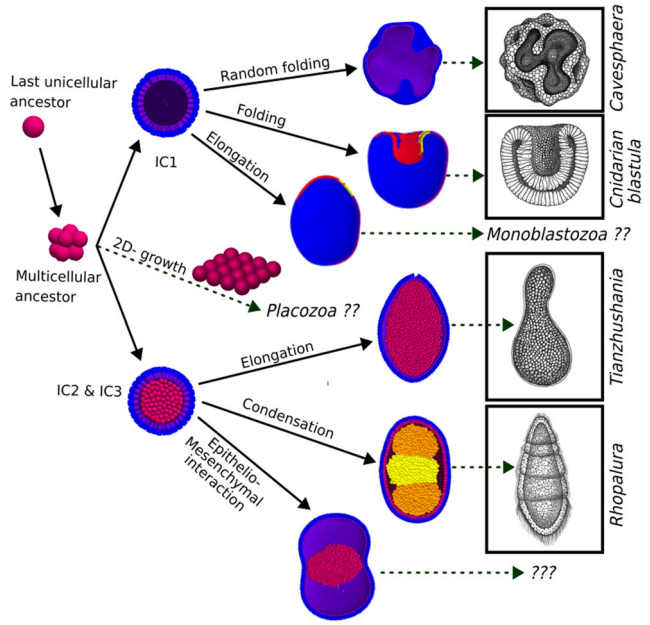

FIGURE 9 | Comparing the morphologies resulting from the ensemble and focal simulations with some Ediacaran fossils and early developmental stages of animals. From left to right: the last unicellular and multicellular ancestors of animals represented with spherical cells, the morphologies of the initial conditions of this study, and some of the morphologies obtained in the simulations by folding, elongation, condensation and interactions between epithelial (in blue and purple) and mesenchymal (in red) cells. Solid lines represent developmental transformations while dotted lines represent plausible developmental origins of known morphologies that our study suggests. The drawings in the right show several organisms from Ediacaran fossils (*Caveasphera, Tianzhushania*) and from extant taxa (a cnidarian blastula, an archetypical Monoblastozoa and the mesozoan *Rhopalura*) whose morphologies can be easily derived by combining basic morphogenetic mechanisms. Original drawings by M.B.-U.

EmbryoMaker. However, they were not observed in our simulations because we did not simulated epithelio-mesenchymal transition and, therefore, cells were not able detach from the epithelium.

The fossils of *Caveasphaera* (Xiao and Knoll 2000) and *Eocyathispongia* (Yin et al. 2015), from the Weng'an biota show morphologies with folds that seem to be randomly distributed, like the ones obtained in our focal approach simulations where the only involved cell behavior regulated was cell division (Figure 9). In a recent article we further explained why epithelia fold randomly when growing by cell division (Cano-Fernández et al. 2024). Another study using EmbryoMaker has already shown that the activation of cell properties and behaviors, such as cell division or cell contraction in all the cells of the embryo, or at least in a large territory, leads to randomly folded morphologies (Hagolani et al. 2019). This means that spatial heterogeneity in gene expression or in environmental conditions is not actually required for morphogenesis, only for given morphologies to be reliable produced in spite of developmental noise. Morphogenesis only requires the presence of multiple cells that are able to change their properties or perform behaviors and that interact physically with each other by adhesion and repulsion forces. This supports the idea that morphogenesis is inherent to multicellular organisms (Newman, Forgacs, and Muller 2006).

Nevertheless, our simulations do not match completely the morphology and development of *Eocyathispongia* and *Caveasphaera*. For example, *Eocyathispongia*, which has been interpreted as an early poriferan, presents multiple inner cavities that are not observed in our simulations (Yin et al. 2015). Multiple cavities were not possible in our simulations because, at is has been mentioned before, we did not allow the epithelium to break or fuse.

The reconstruction of the development of *Caveasphaera* based on morphological data does not completely match with our simulations either. The paleontological reconstruction suggests that cells in *Caveasphaera* were enclosed by a spherical envelope and they grew from an eccentric point to fill all the internal volume (Yin et al. 2019). Conversely, our blastuloids were not constrained physically by any external envelope and growth happened in all directions.

Our simulations also show elongated morphologies that resemble the fossil *Tianzhushania* from the Weng'an biota (Huldtgren et al. 2011) or to some simple animals such as *Rhopalura* (Figure 9) (Slyusarev, Skalon, and Starunov 2022, 2023). It is unclear, however, whether *Tianzhushania* can be associated to animals at all (Moczydłowska and Liu 2022) and the simplified morphology of the parasite *Rhopalura* is probably derived.

The fact that some of our simulations resemble the morphologies of fossils from the Ediacaran period opens the possibility to reconstruct the morphologies of early animals, as well as their development. Some studies have reconstructed the process of development in extinct animals comparing fossils from the same species but in different developmental stages (Yin et al. 2013, 2019, 2020, 2022; Evans, Droser, and Gehling 2017; Hoekzema et al. 2017). Their results are evidence-based descriptions of morphogenetic transformations that, however, do not aim to explain their underlying cellular processes.

Other studies have used simple models that implement cell movement, division, adhesion and signaling to study the processes underlying animal multicellularity (Hogeweg 2000; Mora Van Cauwelaert et al. 2015; Colizzi, Vroomans, and Merks 2020; Japón, Jiménez-Morales, and Casares 2022; Vroomans and Colizzi 2023). These studies, however, were two dimensional (but see Japón, Jiménez-Morales and Casares 2022) and lacked many cell properties and behaviors that are implemented in EmbryoMaker.

The present study has obtained a set of the most basic morphologies that can be produced by animal development using simple assumptions about the initial conditions and genetic territories. Previous theoretical work had already described some of these morphologies that can emerge from simple biophysical rules and environmental heterogeneities (Newman 1994; Newman and Müller 2000), but we have obtained them using a general mathematical model of development. Importantly, we show that some morphogenetic

transformations are only possible in the presence of specific cell behaviors. For example, elongation in the epithelium only happens due to planar cell contraction (Table 1). Many of the cell properties and behaviors considered in this study were not present in the first multicellular animals, but appeared later in evolution. What properties and behaviors were cells able to regulate, therefore, has probably determined what morphological transformations, and thus morphologies, have been likely, or even possible, to appear during animal evolution, as proposed by previous work (Newman and Bhat 2008, 2009).

The present work opens the possibility to perform development-based reconstructions of early multicellular animals. This development-based reconstruction would allow us to propose explanations about how fossil morphologies may have developed and, potentially, suggest the morphologies of extinct animals that are not represented in the fossil record. These more specific reconstructions, however, will need further information about the initial conditions of development and the properties and behaviors that cells were able to regulate in the organisms of interest.

Acknowledgments

We thank Aleksa Ratarac, Antonio Loreto Velázquez, Junya Watanabe, Kevin Martínez Anhon, Hugo Martín Abad, Sergio Martínez Nebreda and Jesus Marugan Lobon for their comments. We are also grateful to the Spanish Super-computing Network (RES) for granting us access to the high performance computers that were required for our simulations. We thank the Spanish Ministry of Science and Innovation for funding (PID2021-122930NB-I00 and CNS2022-135397) to I.S.-C. and FPU19/01428 to H.C.-F. This work was also supported by the Spanish State Research Agency, through the Severo Ochoa and María de Maeztu Program for Centers and Units of Excellence in R&D (CEX2020-001084-M) to the Centre de Recerca Matemàtica.

Data Availability Statement

The last version of the model EmbryoMaker is freely available online, the initial condition files used in the simulations of this article and the code needed to reconstruct all the simulations in our ensembles can be found in the online repository: https://github.com/HugoCanoFernandez/Morphospace_exploration_EMaker.

Peer Review

The peer review history for this article is available at https://www.webofscience.com/api/gateway/wos/peer-review/10.1002/jez.b.23279.

References

Alberch, P. 1991. "From Genes to Phenotype: Dynamical Systems and Evolvability." *Genetica* 84: 5–11.

Burke, R. D., R. L. Myers, T. L. Sexton, and C. Jackson. 1991. "Cell Movements During the Initial Phase of Gastrulation in the Sea Urchin Embryo." *Developmental Biology* 146: 542–557.

Cano-Fernández, H., T. Tissot, M. Brun-Usan, and I. Salazar-Ciudad. 2023. "On the Origins of Developmental Robustness: Modeling Buffering Mechanisms Against Cell-Level Noise." *Development* 150: dev201911.

Cano-Fernández, H., T. Tissot, M. Brun-Usan, and I. Salazar-Ciudad. 2024. "A Mathematical Model of Development Shows That Cell Division, Short-Range Signaling and Self-Activating Gene Networks Increase Developmental Noise While Long-Range Signaling and Epithelial Stiffness Reduce It." *Scientific Journal (Under Review).*

Colizzi, E. S., R. M. Vroomans, and R. M. Merks. 2020. "Evolution of Multicellularity by Collective Integration of Spatial Information." *eLife* 9: e56349.

Davidson, L. A., M. A. R. Koehl, R. Keller, and G. F. Oster. 1995. "How Do Sea Urchins Invaginate? Using Biomechanics to Distinguish Between Mechanisms of Primary Invagination." *Development* 121: 2005–2018.

Evans, S. D., M. L. Droser, and J. G. Gehling. 2017. "Highly Regulated Growth and Development of the Ediacara Macrofossil *Dickinsonia costata*." *PLoS One* 12: e0176874.

Foty, R. A., and M. S. Steinberg. 2005. "The Differential Adhesion Hypothesis: A Direct Evaluation." *Developmental Biology* 278: 255–263.

Gilbert, S. F. 2019. *Developmental Biology*. Sunderland: Sinauer Associates, Inc.

Hagolani, P. F., R. Zimm, M. Marin-Riera, and I. Salazar-Ciudad. 2019. "Cell Signaling Stabilizes Morphogenesis Against Noise." *Development* 146: dev179309.

Hoekzema, R. S., M. D. Brasier, F. S. Dunn, and A. G. Liu. 2017. "Quantitative Study of Developmental Biology Confirms *Dickinsonia* as a Metazoan." *Proceedings of the Royal Society B: Biological Sciences* 284: 20171348.

Hogeweg, P. 2000. "Evolving Mechanisms of Morphogenesis: On the Interplay Between Differential Adhesion and Cell Differentiation." *Journal of Theoretical Biology* 203: 317–333.

Huldtgren, T., J. A. Cunningham, C. Yin, et al. 2011. "Fossilized Nuclei and Germination Structures Identify Ediacaran "Animal Embryos" as Encysting Protists." *Science* 334: 1696–1699.

Japón, P., F. Jiménez-Morales, and F. Casares. 2022. "Intercellular Communication and the Organization of Simple Multicellular Animals." *Cells & Development* 169: 203726.

Lecuit, T., and P.-F. Lenne. 2007. "Cell Surface Mechanics and the Control of Cell Shape, Tissue Patterns and Morphogenesis." *Nature Reviews Molecular Cell Biology* 8: 633–644.

Mammoto, T., A. Mammoto, Y. Torisawa, et al. 2011. "Mechanochemical Control of Mesenchymal Condensation and Embryonic Tooth Organ Formation." *Developmental Cell* 21: 758–769.

Marin-Riera, M., M. Brun-Usan, R. Zimm, T. Välikangas, and I. Salazar-Ciudad. 2015. "Computational Modeling of Development by Epithelia, Mesenchyme and Their Interactions: A Unified Model." *Bioinformatics* 32: 219–225.

Marin-Riera, M., J. Moustakas-Verho, Y. Savriama, J. Jernvall, and I. Salazar-Ciudad. 2018. "Differential Tissue Growth and Cell Adhesion Alone Drive Early Tooth Morphogenesis: An Ex Vivo and in Silico Study." *PLoS Computational Biology* 14: e1005981.

Martin, A. C., M. Kaschube, and E. F. Wieschaus. 2009. "Pulsed Contractions of an Actin–Myosin Network Drive Apical Constriction." *Nature* 457: 495–499.

McGhee, G. R. 2011. *Convergent Evolution: Limited Forms Most Beautiful*. Cambridge MA: MIT Press.

Moczydłowska, M., and P. Liu. 2022. "Ediacaran Algal Cysts From the Doushantuo Formation, South China." *Geological Magazine* 159: 1050–1070.

Monier, B., M. Gettings, G. Gay, et al. 2015. "Apico-Basal Forces Exerted by Apoptotic Cells Drive Epithelium Folding." *Nature* 518: 245–248.

Mora Van Cauwelaert, E., J. A. Arias Del Angel, M. Benítez, and E. M. Azpeitia. 2015. "Development of Cell Differentiation in the Transition to Multicellularity: A Dynamical Modeling Approach." *Frontiers in Microbiology* 6: 603.

Newman, S. A. 1994. "Generic Physical Mechanisms of Tissue Morphogenesis: A Common Basis for Development and Evolution." *Journal of Evolutionary Biology* 7: 467–488.

Newman, S. A. 1996. “Sticky Fingers: Hox Genes and Cell Adhesion in Vertebrate Limb Development.” *BioEssays* 18: 171–174.

Newman, S. A., and R. Bhat. 2008. “Dynamical Patterning Modules: Physico-Genetic Determinants of Morphological Development and Evolution.” *Physical Biology* 5: 015008.

Newman, S. A., and R. Bhat. 2009. “Dynamical Patterning Modules: A “Pattern Language” for Development and Evolution of Multicellular Form.” *The International Journal of Developmental Biology* 53: 693–705.

Newman, S. A., G. Forgacs, and G. B. Muller. 2006. “Before Programs: The Physical Origination of Multicellular Forms.” *The International Journal of Developmental Biology* 50: 289–299.

Newman, S. A., and G. B. Müller. 2000. “Epigenetic Mechanisms of Character Origination.” *Journal of Experimental Zoology* 288: 304–317.

Pearl, E. J., J. Li, and J. B. A. Green. 2017. “Cellular Systems for Epithelial Invagination.” *Philosophical Transactions of the Royal Society, B: Biological Sciences* 372: 20150526.

Salazar-Ciudad, I. 2006. “On the Origins of Morphological Disparity and Its Diverse Developmental Bases.” *BioEssays* 28: 1112–1122.

Salazar-Ciudad, I. 2010. “Morphological Evolution and Embryonic Developmental Diversity in Metazoa.” *Development* 137: 531–539.

Salazar-Ciudad, I., J. Garcia-Fernández, and R. V. Solé. 2000. “Gene Networks Capable of Pattern Formation: From Induction to Reaction–Diffusion.” *Journal of Theoretical Biology* 205: 587–603.

Salazar-Ciudad, I., J. Jernvall, and S. A. Newman. 2003. “Mechanisms of Pattern Formation in Development and Evolution.” *Development* 130: 2027–2037.

Salazar-Ciudad, I., and H. Cano-Fernández. 2023. “Evo-Devo Beyond Development: Generalizing Evo-Devo to All Levels of the Phenotypic Evolution.” *BioEssays* 45: 2200205.

Sherrard, K., F. Robin, P. Lemaire, and E. Munro. 2010. “Sequential Activation of Apical and Basolateral Contractility Drives Ascidian Endoderm Invagination.” *Current Biology* 20: 1499–1510.

Slyusarev, G. S., N. I. Bondarenko, E. K. Skalon, A. K. Rappoport, D. Radchenko, and V. V. Starunov. 2022. “The Structure of the Muscular and Nervous Systems of the Orthonectid *Rhopalura litoralis* (Orthonectida) or What Parasitism Can Do to an Annelid.” *Organisms Diversity & Evolution* 22: 35–45.

Slyusarev, G. S., E. K. Skalon, and V. V. Starunov. 2023. “Evolution of Orthonectida Body Plan.” *Evolution & Development* 26, no. 4: e12462.

Steinberg, M. S. 1970. “Does Differential Adhesion Govern Self-Assembly Processes in Histogenesis? Equilibrium Configurations and the Emergence of a Hierarchy Among Populations of Embryonic Cells.” *Journal of Experimental Zoology* 173: 395–433.

Taylor, H. B., A. Khuong, Z. Wu, et al. 2017. “Cell Segregation and Border Sharpening by Eph Receptor–Ephrin-Mediated Heterotypic Repulsion.” *Journal of the Royal Society Interface* 14: 20170338.

Technau, U. 2020. “Gastrulation and Germ Layer Formation in the Sea Anemone *Nematostella Vectensis* and Other Cnidarians.” *Mechanisms of Development* 163: 103628.

True, J. R., and E. S. Haag. 2001. “Developmental System Drift and Flexibility in Evolutionary Trajectories.” *Evolution & Development* 3: 109–119.

Vroomans, R. M. A., and E. S. Colizzi. 2023. “Evolution of Selfish Multicellularity: Collective Organisation of Individual Spatio-Temporal Regulatory Strategies.” *BMC Ecology and Evolution* 23: 35.

Wang, Y., D. Stonehouse-Smith, M. T. Cobourne, J. B. A. Green, and M. Seppala. 2022. “Cellular Mechanisms of Reverse Epithelial Curvature in Tissue Morphogenesis.” *Frontiers in Cell and Developmental Biology* 10: 1066399.

Xiao, S., and A. H. Knoll. 2000. “Phosphatized Animal Embryos From the Neoproterozoic Doushantuo Formation at Weng'an, Guizhou, South China.” *Journal of Paleontology* 74: 767–788.

Yin, Z., W. Sun, P. Liu, et al. 2022. “Diverse and Complex Developmental Mechanisms of Early Ediacaran Embryo-Like Fossils From the Weng'an Biota, Southwest China.” *Philosophical Transactions of the Royal Society, B: Biological Sciences* 377: 20210032.

Yin, Z., W. Sun, P. Liu, M. Zhu, and P. C. J. Donoghue. 2020. “Developmental Biology of *Helicoforamina* Reveals Holozoan Affinity, Cryptic Diversity, and Adaptation to Heterogeneous Environments in the Early Ediacaran Weng'an Biota (Doushantuo Formation, South China).” *Science Advances* 6: eabb0083.

Yin, Z., K. Vargas, J. Cunningham, et al. 2019. “The Early Ediacaran *Caveasphaera* Foreshadows the Evolutionary Origin of Animal-Like Embryology.” *Current Biology* 29: 4307–4314.e2.

Yin, Z., M. Zhu, E. H. Davidson, D. J. Bottjer, F. Zhao, and P. Tafforeau. 2015. “Sponge Grade Body Fossil With Cellular Resolution Dating 60 Myr Before the Cambrian.” *Proceedings of the National Academy of Sciences* 112: E1453–E1460.

Yin, Z., M. Zhu, P. Tafforeau, J. Chen, P. Liu, and G. Li. 2013. “Early Embryogenesis of Potential Bilaterian Animals With Polar Lobe Formation From the Ediacaran Weng'an Biota, South China.” *Precambrian Research* 225: 44–57.

Supporting Information

Additional supporting information can be found online in the Supporting Information section.